materials

MDPI

Article

Effect of Chopped ZrO_2 Fiber Content on the Microstructure and Properties of CaO-Based Integral Ceramic Mold

Qiang Yang, Fu Wang * and Dichen Li

State Key Laboratory for Manufacturing System Engineering, School of Mechanical Engineering, Xi'an Jiaotong University, Xi'an 710049, China; yangqiang@stu.xjtu.edu.cn (Q.Y.); xjtudcli@sina.com (D.L.)

* Correspondence: fuwang@xjtu.edu.cn

Received: 19 October 2020; Accepted: 24 November 2020; Published: 27 November 2020

Abstract: A chopped ZrO_2 fiber ($ZrO_{2\ (f)}$) reinforced CaO-based integral ceramic mold was successfully fabricated by stereolithography (SLA) and tert-butyl alcohol (TBA)-based gel-casting, and the effect of chopped $ZrO_{2\ (f)}$ content on properties of the ceramic mold was investigated. The results show that the $ZrO_{2\ (f)}$ content had a significant effect on the viscosity of CaO-based ceramic slurry, which directly affects the filling ability of slurry in complex structures of the integral mold. The tiny structures of the ceramic mold cannot be filled completely with a $ZrO_{2\ (f)}$ content exceeding 3 vol %. The sample fabricated with 3 vol % fiber content showed a harmonious microstructure and exhibited an excellent comprehensive performance with 25 °C bending strength of 22.88 MPa, an 1200 °C bending strength of 15.74 MPa, a 1200 °C deflection of 0.86 mm, and a sintering shrinkage of 0.40%, which can meet the requirements of casting very well.

Keywords: ZrO_2 fiber; calcium oxide; gel-casting; microstructure; properties

1. Introduction

CaO has long been considered an attractive refractory for application in metallurgical and ceramics industries because of the global abundant sources of high-purity limestone, as well as its advantages of high melting temperature, low vapor pressure, and excellent thermodynamic stability [1–5]. In recent years, CaO was studied as a potential ceramic core material for investment casting due to the reaction-resistance to molten active alloy [6–8], easy dissolution compared to common ceramic core materials, such as fused silica or alumina [9–11], and its approximating the thermal expansion coefficient of superalloys [12]. However, in spite of these primary advantageous properties, the application of CaO is inhibited due to its hydration susceptibility in atmospheric moisture [2–5,13,14], which increased the difficultly of fabricating CaO ceramics as well. Most existing methods for forming CaO ceramic, such as hot-pressing [1] and cold-pressing [3–5], can only fabricate simple architectures, which makes them untenable for generating complex ceramic structures.

The rapid integral fabrication technique (RIFT), based on stereolithography (SLA) and non-aqueous gel-casting technology, provides a new approach for fabricating complex ceramic components, especially the ceramic molds of hollow turbine blades [15–18]. Tert-butyl alcohol (TBA) is selected as solvent, on the one hand because it can effectively avoid the hydrolysis of CaO powder, and on the other hand because of its high saturation vapor pressure and low surface tension force: the green body can be easily dried with a small shrinkage and deformation [19]. In order to meet the requirement of investment casting, the ceramic mold must has a good performance in mechanical properties and no structure defects, such as cracks, severe deflection, or shrinkage deformation. However, cracking often occurs during the pre-sintering of the RIFT process. In this stage, the integrity of the ceramic mold can

be only maintained by the particle packing effects because the gel networks were burnt off. Therefore, the slender structures may be broken by gravity and the thin-wall structures also may be broken by the stress caused by pyrolysis of the resin prototype. Moreover, the integral ceramic mold always has slightly poor mechanical properties, a lager deflection, and sintering shrinkage. The unacceptable drawbacks for investment casting of ceramic mold can be overcome by incorporating particulate, whisker, or fiber into the base materials to form ceramic matrix composites [20,21]. Especially using chopped fibers, the ceramic can not only be strengthened in isotropic properties due to the homogenous distribution, but also the ceramic mold with complex structures can be formed by conventional manufacturing techniques, such as slip casting or gel-casting [22,23].

In this work, the chopped $ZrO_{2\,(f)}$ was selected to reinforce the CaO-based integral ceramic mold due to its high melting point, excellent strength and toughness, low thermal conductivity, super corrosion, and oxidation resistance [24]. In addition, the chopped $ZrO_{2\,(f)}$ can be well retained during the sintering of the CaO matrix, because it does not react with the CaO matrix at the lower sintering temperature unlike the silica or alumina fibers. The CaO-based integral ceramic molds are fabricated by the RIFT technique with the TBA-based gel-casting. The effects of chopped $ZrO_{2\,(f)}$ content on the viscosities and filling ability of the slurries, the microstructures, mechanical properties, deflection, and sintering shrinkage of ceramic mold were investigated, and the reinforcing mechanism of chopped $ZrO_{2\,(f)}$ reinforced porous CaO ceramic mold is also discussed.

2. Material and Methods

2.1. Raw Materials

Commercial CaO powders (purity ≥99%, Xing Tai special ceramics Co. Ltd., Xi'an, China), commercial fused MgO powders (Henghai magnesium industry Co., Ltd., Lianyungang, China), and chopped ZrO_2 fiber (mean diameter and length are 5~8 μm and 200 μm, respectively, purity ≥99%, Shandong Huolong Ceramic Fiber Co., Ltd., Jinan, China) were used as the raw materials. Zirconium powder (AR, Western BaoDe Technologies Co., Ltd., Xi'an, China) with a mean particle diameter of 5 μm was used as the sintering additive. The morphology of the CaO powders, MgO powders, and $ZrO_{2\,(f)}$, the particle size distribution of the CaO powders, MgO powders, and the aspect ratio of $ZrO_{2\,(f)}$ are shown in Figure 1.

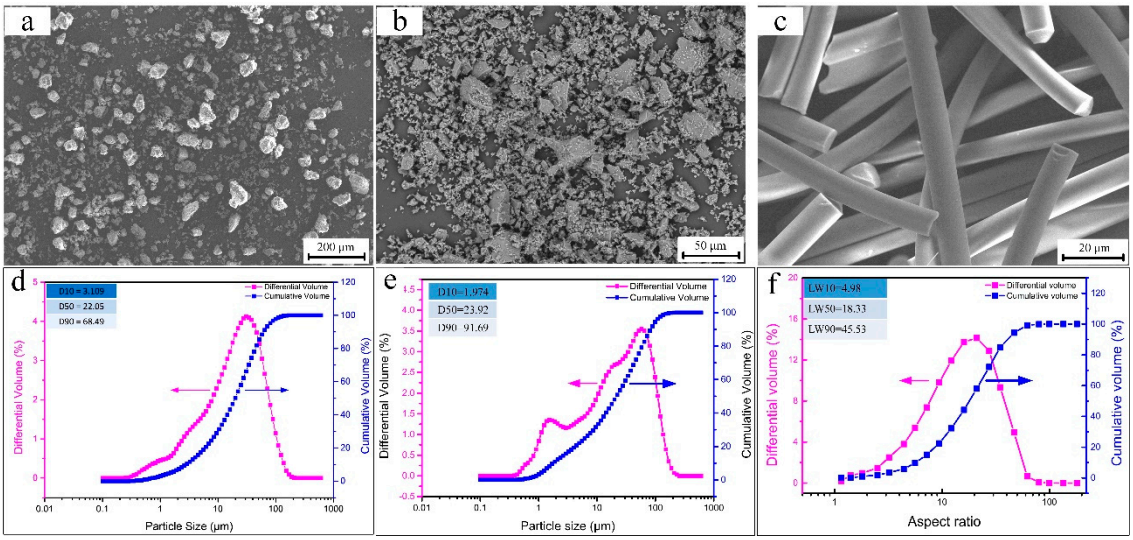

Figure 1. (**a**) SEM micrograph of the CaO powders, (**b**) SEM micrograph of the MgO powders, (**c**) SEM micrograph of the $ZrO_{2\,(f)}$, (**d**) particle size distribution of the CaO powders, (**e**) particle size distribution of the MgO powders, (**f**) aspect ratio of $ZrO_{2\,(f)}$.

2.2. Experimental Procedure

The rapid integral fabrication technique was applied to fabricate the CaO-based ceramic samples and molds, the fabrication flow chart was shown in Figure 2. The premixed solution was prepared by dissolving N, N-dimethylacrylamide (DMAA) and N, N-methylene diacrylamide (MBAM) into the Tert-butyl alcohol (TBA) with the weight ratio of DMAA:MBAM:TBA = 24:2:100. 3 wt.% polyvinyl pyrrolidone (PVP K30) with respect to the total mass of powders was added into the premixed solution as dispersant. All the chemical reagents are of AR purity and provided by Sinopharm Chemical Reagent Ltd., Shanghai, China. Due to the serious agglomeration of the chopped zirconia fibers, the $ZrO_{2\,(f)}$ must be pre-dispersed before use. The $ZrO_{2\,(f)}$ needs to be added into absolute ethyl alcohol, subsequently placed in an ultrasonic disperser for 2–4 h, and dried finally. Then the appropriate amount of CaO, MgO, and Zirconium powders and a certain amount of processed $ZrO_{2\,(f)}$ were added into the premixed solution by mechanical stirring, followed by the ball milling for 50~60 min. The prepared slurries exhibited a good flow-ability and stability and were degased for more than 5 min. After adding an appropriate amount of N,N-dimethylaniline (DMA) as initiator and benzoyl peroxide (BPO) as catalyst, the mixed slurry was poured into the SLA resin mold fabricated by SPS600B Rapid Prototyping Machine (Shaanxi Hengtong Intelligent Machine Co., Ltd., Xi'an, China) using photosensitive resin (SPR 8981; Zheng bang Ltd., Zhuhai, China) under vacuum and vibration conditions. After the polymerization of the monomers, the green body was put into the vacuum drying oven (Taisite Instrument Co., Ltd., Tianjin, China) at 40 °C for 48 h. At last, an integral CaO-based ceramic mold was obtained after being sintered at 1400 °C and kept for 3 h [18]. According to our previous study [18], during the fabrication process, the optimal total solid loading (the solid loading of CaO powder, MgO powder, Zirconium powder, and $ZrO_{2\,(f)}$) of the slurry was fixed at 56 vol %, while the content of $ZrO_{2\,(f)}$ varied from 0 vol % to 4 vol %; the volume fraction is calculated based on the assumption that the packing of powder particles is compact. The component of the composite powders is shown in Table 1.

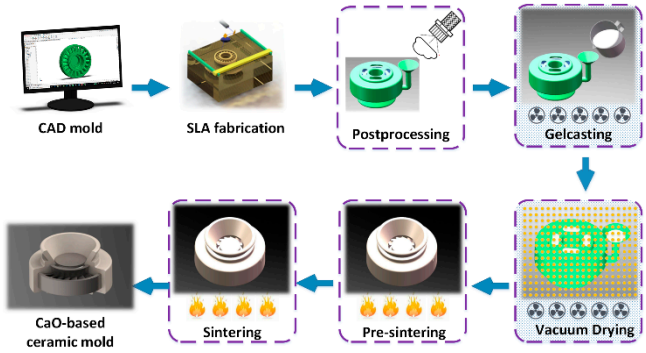

Figure 2. Fabrication flow chart of the CaO-based integral ceramic mold [18].

Table 1. Component of the composite powders.

Sample Number	Volume Fraction (vol %)			
	CaO	MgO	Zr	$ZrO_{2\,(f)}$
A	42.00	12.00	2.00	0.00
B	41.00	12.00	2.00	1.00
C	40.00	12.00	2.00	2.00
D	39.00	12.00	2.00	3.00
E	38.00	12.00	2.00	4.00

2.3. Characterization and Testing

The particle sizes of the powders were measured by the Laser Particle Sizer (BT-9300S, Better Instruments Co., Ltd., Dandong, China). The viscosity of CaO-based ceramic slurries was tested by

the Digital rotational viscometer (SNB-3, Shanghai NiRun Intelligent Technology Co., Ltd., Shanghai, China). The structures of the samples and the integral ceramic molds were investigated by the micro X-ray imaging system (industrial CT) (Y. Cheetah, YXLON, Hamburg, Germany) with a scanning resolution of 50 μm. The phase composition was identified by X-ray diffraction (XRD) (X'Pert Protype, PANalytical BV, Almelo, The Netherlands). The microstructure and elemental composition of samples were investigated by the field emission scanning electron microscope (SEM) (SU-8010, Hitachi Ltd., Tokyo, Japan). The bending strengths of samples were tested by a three-point bending test machine (HSST-6003QP, Sinosteel Luoyang Institute of Refractories, Luoyang, China) with a span distance of 30 mm at a crosshead speed of 6 mm/min using samples of a nominal size of 4 mm × 10 mm × 60 mm. The apparent porosity of sintered bodies were measured by immersion method in absolute ethyl alcohol under vacuum using Archimedes' principle. The sintering shrinkage of samples was calculated according to the following Equation (1).

$$\varepsilon = \frac{L_1 - L_2}{L_1} \times 100\% \quad (1)$$

where ε is the shrinkage of sample, L_1 is the length of sample before sintering, L_2 is the length of sample after sintering.

3. Result and Discuss

3.1. Effect on Viscosity and Filling Ability of the Slurry

It is always very difficult to fill the tiny and complex structures in the ceramic mold sufficiently during the fabrication process of the integral ceramic mold by RIFT process, as shown in Figure 3a. Some insufficient filled situations often occur in these tiny structures, which leads to the loss of the structural integrity of the mold and the failure of ceramic mold fabrication. The structural integrity of the ceramic mold is directly determined by the filling ability of the ceramic slurry, depending on the viscosity of the ceramic slurry. Generally speaking, in order to obtain a complete filling of the fine structure, the viscosity of the ceramic slurry is must less than 1 Pa s in the gel-casting process [17]. Since the viscosity of ceramic slurry is very sensitive to the content of $ZrO_{2\,(f)}$, it is very important to obtain an appropriate $ZrO_{2\,(f)}$ addition amount to realize the tiny structures duplication without defects.

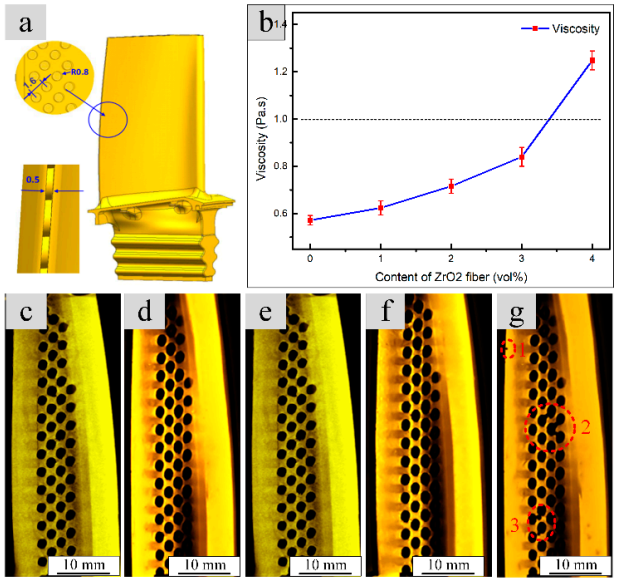

Figure 3. Effects of $ZrO_{2\,(f)}$ content on viscosity and filling ability of the slurries: (**a**) schematic of tiny and complex structures in the ceramic mold, (**b**) viscosity of slurries with different $ZrO_{2\,(f)}$ content, (**c**–**g**) CT images of different $ZrO_{2\,(f)}$ content: (**c**) 0 vol %, (**d**) 1 vol %, (**e**) 2 vol %, (**f**) 3 vol %, (**g**) 4 vol %.

Figure 3b–g shows the effect of $ZrO_{2\,(f)}$ content on viscosity and filling ability of the slurries. As can be seen from Figure 3b, the viscosity of slurries increased gradually with the increasing of $ZrO_{2\,(f)}$ content. When the $ZrO_{2\,(f)}$ content reaches 4 vol %, the viscosity exceed 1Pa·s, the limit of slurry viscosity in gel-casting process. As shown in Figure 3c–g, the tiny structures could be filled perfectly, when the $ZrO_{2\,(f)}$ content was not exceeding 3 vol %. However, some insufficient filled areas were found in the tiny structures as the $ZrO_{2\,(f)}$ content further increase to 4 vol %, as shown in Figure 3g (area 1, 2, 3). This phenomenon is mainly caused by the high viscosity (>1 Pa·s) of ceramic slurry, due to the addition of excessive fibers. Therefore, in order to guarantee that the tiny structures can be filled completely by the CaO-based ceramic slurry with a low viscosity, the $ZrO_{2\,(f)}$ content cannot exceed 3 vol % in the RIFT process to fabricate the ceramic mold with complex structures.

3.2. Microstructure and Phase Analysis

Figure 4a–d shows the fracture surface of the samples fabricated with different $ZrO_{2\,(f)}$ additions after sintered at 1400 °C for 3 h. As shown in Figure 4a–c, the $ZrO_{2\,(f)}$ are randomly arranged and homogeneously distributed in the CaO ceramic matrix when the content is not exceeding 3 vol %; whereas, the $ZrO_{2\,(f)}$ are likely to distribute in fasciculate when the content is up to 4 vol %, as shown in Figure 4d. The heterogeneous distribution of $ZrO_{2\,(f)}$ is caused by the insufficient dispersion of excess fiber in slurry. It can be noticed that the fibers length in the final composite are 60~70 μm on average, far shorter than the raw $ZrO_{2\,(f)}$, mainly caused by worn during the ball milling. In fact, in order to achieve better reinforcement, the damage to chopped fibers should be avoided. However, the ball milling, an effective and simple dispersion approach, is widely used for dispersion of high solid loading slurry with chopped fibers, which leads to the inevitable damage to chopped fibers. Therefore, it is very important to optimize the ball milling process, especially the duration of ball milling. In this study, the duration of ball milling is controlled in 40 min, to obtain a well-dispersed slurry without the severe damage of fibers.

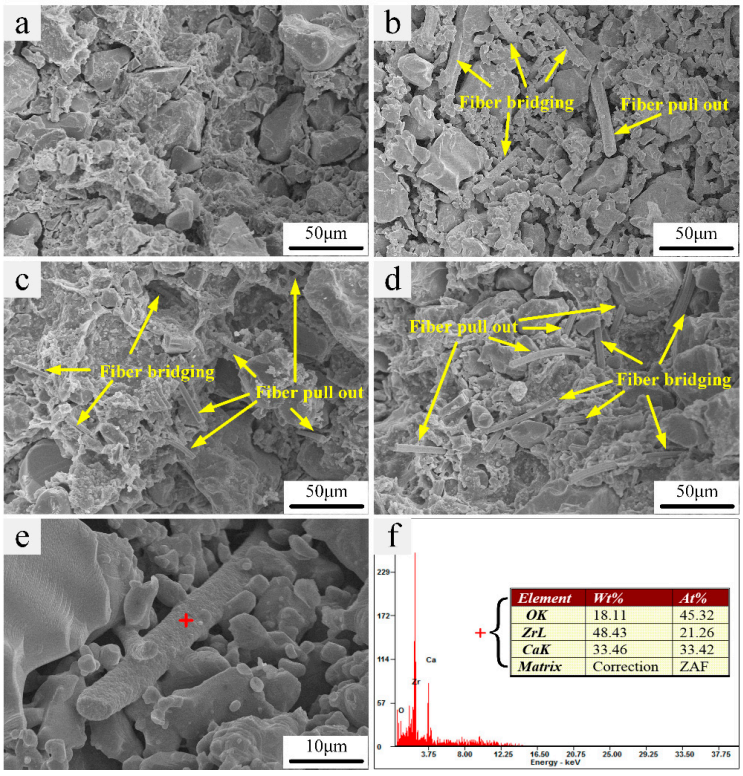

Figure 4. SEM micrographs of fracture surface with different $ZrO_{2\,(f)}$ content: (**a**) 1 vol %, (**b**) 2 vol %, (**c**) 3 vol %, (**d**) 4 vol %, (**e**,**f**) EDS of $ZrO_{2\,(f)}$ interface.

The primary toughening mechanism of the chopped fiber reinforced ceramic matrix composite is the fiber pulling-out, bridging, and deboning. The fiber pulling-out and bridging can be obviously observed in Figure 4a–d, and the deboning can be observed in Figure 4e. The EDS was carried out to identify the composition on the interface of fiber and CaO matrix. According to the proportion of the elements distribution, as shown in Figure 4f, it can be inferred that the main component of the interface on the fiber may be the calcium zirconate ($CaZrO_3$), formed by the reaction of CaO and ZrO_2 at elevated temperature, as shown in Equation (2). It indicates that a strong interface is formed on the surface of fibers, which could transfer the load effectively and reinforce the mechanical properties. In addition, the layer of $CaZrO_3$ on the surface of $ZrO_{2\,(f)}$ fiber will also protect the internal $ZrO_{2\,(f)}$, preventing the further reaction of $ZrO_{2\,(f)}$ and the CaO matrix at an elevated temperature.

$$CaO + ZrO_2 \triangleq CaZrO_3 \quad (2)$$

Figure 5 shows the XRD pattern of the sintered CaO-based ceramic mold with different content of $ZrO_{2\,(f)}$. As can be seen, these patterns are dominated by the diffraction peaks of CaO, MgO, $CaZrO_3$, and ZrO_2. The diffraction peaks of CaO and MgO should be determined by the raw materials of CaO and MgO in the ceramic matrix. The diffraction peaks of ZrO_2 should be the characteristic of $ZrO_{2\,(f)}$, because the zirconium powder added to the matrix material is easily oxidized to ZrO_2 when the green body is sintered in the atmosphere, then reacts with the CaO matrix to form a $CaZrO_3$ phase, and there is no other source of ZrO_2. In addition, the peak intensity of ZrO_2 gradually increased with the increase of the content of $ZrO_{2\,(f)}$, indicating that the ZrO_2 phase in the ceramic mold mainly comes from $ZrO_{2\,(f)}$, and the $ZrO_{2\,(f)}$ still existed as fiber, although the surface of the $ZrO_{2\,(f)}$ reacted with the CaO matrix to form a $CaZrO_3$ phase, which is also consistent with the SEM results observed in the microstructure.

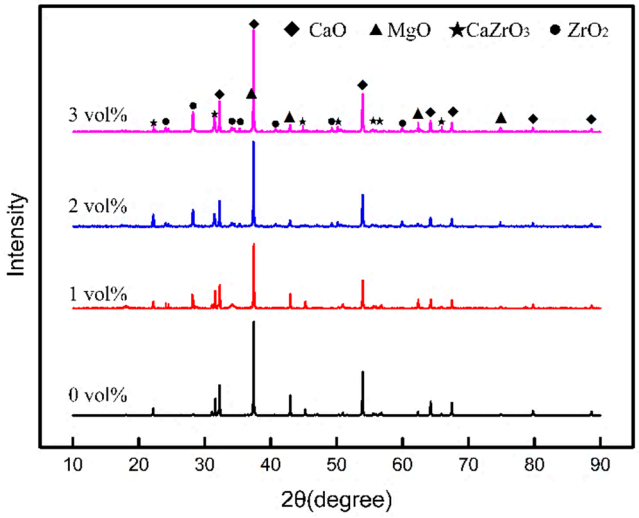

Figure 5. XRD Patterns of sintered ceramic mold with different $ZrO_{2\,(f)}$ content.

3.3. Mechanical Properties and Sintering Shrinkage

Figure 6 shows the mechanical properties and sintering shrinkage of the samples fabricated with different $ZrO_{2\,(f)}$ content after sintered. As can be seen from Figure 6a, both the room temperature (25 °C) and elevated temperature (1200 °C) bending strength increased with the $ZrO_{2\,(f)}$ content varying from 0 vol % to 3 vol % and peaked at 22.88 MPa and 15.74 MPa, respectively, when $ZrO_{2\,(f)}$ content is 3 vol %. Further increase the content of $ZrO_{2\,(f)}$ resulted in a slight decrease of bending strength due to the inhomogeneous microstructure of CaO-based ceramic sample caused by the heterogeneous distribution of excessive $ZrO_{2\,(f)}$. As can be seen from Figure 6b, the elevated temperature (1200 °C) deflection decreased as the $ZrO_{2\,(f)}$ content increased from 0 vol % to 3 vol % and the minimum

deflection is 0.86 mm, when $ZrO_{2\,(f)}$ content is 3 vol %. A slight increase of deflection was exhibited with the further addition of the $ZrO_{2\,(f)}$ caused by the heterogeneous distribution of excessive $ZrO_{2\,(f)}$ as well. As can be seen from Figure 6c,d, the apparent porosity increased from 29.46% to 31.42% and the sintering shrinkage decreased from 0.57% to 0.40% as the $ZrO_{2\,(f)}$ content increased from 1vol% to 3 vol %. It indicates that the chopped $ZrO_{2\,(f)}$ may well be formed in a bracket for the CaO ceramic matrix, and the CaO ceramic particles are fixed to retard the translocation of ceramic particles, so that the porosity of the ceramic mold increased and the sintering shrinkage decreased. It showed that the mechanical properties and the sintering shrinkage could be significantly improved by the addition of $ZrO_{2\,(f)}$.

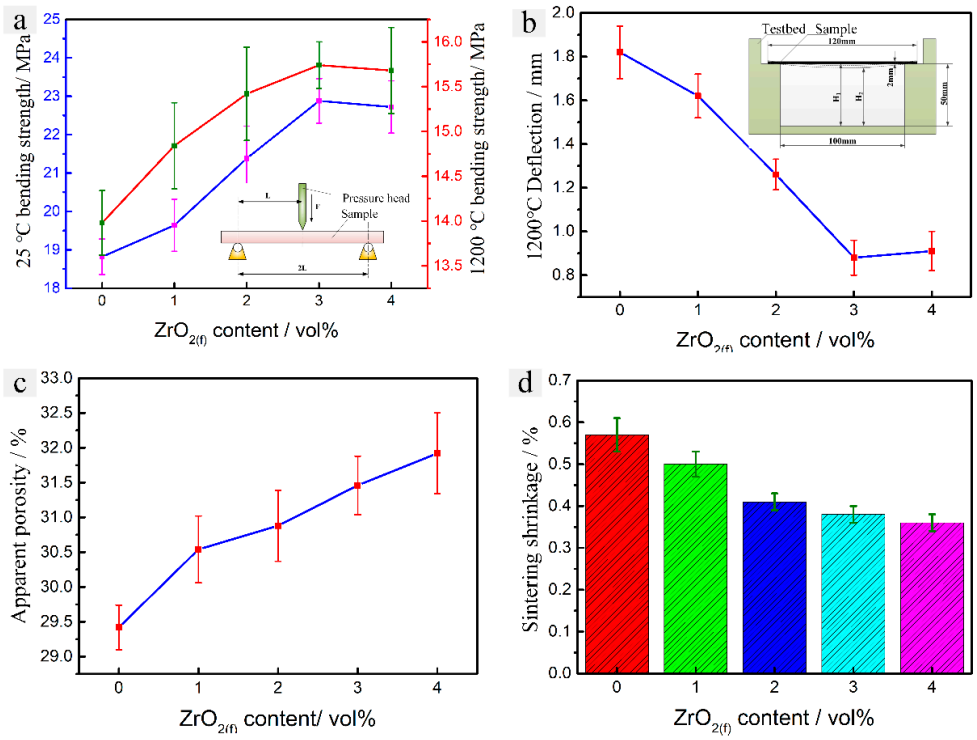

Figure 6. Effect of $ZrO_{2\,(f)}$ content on properties of CaO-based ceramic mold: (**a**) room and elevated temperature (1200 °C) bending strength, (**b**) deflection (1200 °C), (**c**) apparent porosity, (**d**) sintering shrinkage.

3.4. Case Study

A CaO-based ceramic mold of impeller was fabricated by the RIFT with the $ZrO_{2\,(f)}$ content of 3 vol % according to the procedure described in Section 2, as shown in Figure 7a–d and the internal structure of the mold was tested by industrial CT, as shown in Figure 7e–h. X-ray analysis reveals that the shape of the impeller was exactly duplicated and the internal structure of the impeller ceramic mold was well maintained, indicating that the CaO-based ceramic mold reinforced by chopped $ZrO_{2\,(f)}$ can meet the requirements of casting.

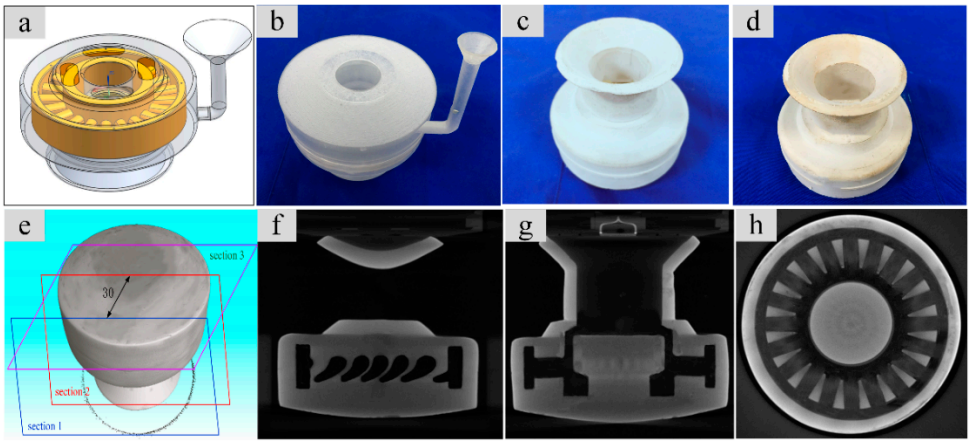

Figure 7. Fabrication of CaO-based ceramic mold of an impeller and the CT image of mold: (**a**) CAD mold, (**b**) resin mold, (**c**) dried green body, (**d**) sintered ceramic mold, (**e**) scan section of CT, (**f**) CT image of Section 1, (**g**) CT image of Section 2, (**h**) CT image of Section 3.

4. Conclusions

A CaO-based integral ceramic mold with improved mechanical properties has been fabricated by SLA and TBA-based gel-casting with the chopped $ZrO_{2\,(f)}$ reinforced method. In order to obtain a sufficiently filled green body of CaO-based integral ceramic mold with tiny structure, the content of $ZrO_{2\,(f)}$ should not exceed 3 vol %. SEM and XRD analysis shows that the sample fabricated with the addition of $ZrO_{2\,(f)}$ content of 3 vol % has a microstructure with a homogeneous distribution of $ZrO_{2\,(f)}$, which reinforces the CaO-based ceramic mold with fiber pulling-out, bridging, and deboning. The room temperature (25 °C) bending strength increased to 22.88 MPa, elevated temperature (1200 °C) bending strength increased to 15.74 MPa, sintering shrinkage decreased to 0.40% and apparent porosity increased to 31.42%, respectively. This CaO-based ceramic mold is an excellence candidate to be used in investment casting for the aerospace and engineering fields.

Author Contributions: Conceptualization, D.L. and Q.Y.; Methodology, Q.Y., F.W., and D.L.; Software, Q.Y.; Validation, Q.Y. and D.L.; Formal Analysis, F.W.; Investigation, Q.Y.; Resources, F.W. and D.L.; Data Curation, F.W.; Writing—Original Draft Preparation, Q.Y.; Writing—Review & Editing, Q.Y.; Visualization, Q.Y.; Supervision, D.L.; Project Administration, F.W.; Funding Acquisition, F.W. All authors have read and agreed to the published version of the manuscript.

Funding: This research was funded by the Key Program of Equipment Pre-Research Foundation of China [Grant No. 61409230405] and the National Natural Science Foundation of China [Grant No. 91860103].

Acknowledgments: The authors gratefully acknowledge the support of the Key Program of Equipment Pre-Research Foundation of China (Grant No. 61409230405) and the National Natural Science Foundation of China (Grant No. 91860103). We thank Zijun Ren at Instrument Analysis Center of Xi'an Jiaotong University for his assistance with SEM and EDS analysis.

Conflicts of Interest: The authors declare no conflict of interest.

References

1. Rice, R.W. CaO: I, Fabrication and characterization. *J. Am. Ceram. Soc.* **1969**, *52*, 420–427. [CrossRef]
2. Li, Z.; Zhang, S.; Lee, W.E. Improving the hydration resistance of lime-based refractory materials. *Int. Mater. Rev.* **2008**, *53*, 1–20. [CrossRef]
3. Ghosh, A.; Bhattacharya, T.; Mukherjee, B.; Das, S. The effect of CuO addition on the sintering of lime. *Ceram. Int.* **2001**, *27*, 201–204. [CrossRef]
4. Ghosh, A.; Bhattacharya, T.; Maiti, S.; Mukherjee, B.; Tripathi, H.; Das, S. Densification and properties of lime with V2O5 additions. *Ceram. Int.* **2004**, *30*, 2117–2120. [CrossRef]
5. Ghasemi-Kahrizsangi, S.; Nemati, A.; Shahraki, A.; Farooghi, M. Densification and properties of Fe2O3 Nanoparticles added CaO refractories. *Ceram. Int.* **2016**, *42*, 12270–12275. [CrossRef]

6. Hung, C.; Lai, P.; Tsai, C.; Huang, T.; Liao, Y. Pure titanium casting into titanium-modified calcia-based and magnesia-based investment molds. *Mater. Sci. Eng. A* **2007**, *454*, 178–182. [CrossRef]
7. Klotz, U.E.; Heiss, T. Evaluation of crucible and investment materials for lost wax investment casting of Ti and NiTi alloys. *Int. J. Cast Met. Res.* **2014**, *27*, 341–348. [CrossRef]
8. Fu, B.-G.; Wang, H.-W.; Zou, C.-M.; Ma, P.; Wei, Z.-J. Interfacial reactions between Ti-1100 alloy and CaO crucible during casting process. *Trans. Nonferrous Met. Soc. China* **2014**, *24*, 3118–3125. [CrossRef]
9. Liu, F.; Fan, Z.; Liu, X.; He, J.; Li, F. Aqueous gel casting of water-soluble calcia-based ceramic core for investment casting using epoxy resin as a binder. *Int. J. Adv. Manuf. Technol.* **2016**, *86*, 1235–1242. [CrossRef]
10. Yang, Q.; Lu, Z.; Huang, F.; Li, D. The Preparation of calcia-based ceramic slurry for rapid manufacturing hollow turbine blade based on stereolithography. In Proceedings of the 2nd International Conference on Progress in AM, Kallang, Singapore, 16–19 May 2016; pp. 158–163.
11. Zhao, H.; Ye, C.; Fan, Z.; Wang, C. 3D printing of CaO-based ceramic core using nanozirconia suspension as a binder. *J. Eur. Ceram. Soc.* **2017**, *37*, 5119–5125. [CrossRef]
12. Hulse, C.O. Process of Casting Nickel Base Alloys Using Water-Soluble Calcia Cores. U.S. Patent 3 643 728, 22 February 1972.
13. Beruto, D.; Barco, L.; Belleri, G.; Searcy, A.W. Vapor-phase hydration of submicrometer CaO particles. *J. Am. Ceram. Soc.* **1981**, *64*, 74–80. [CrossRef]
14. Chen, G.; Li, B.; Zhang, H.; Qin, Z.; Lu, X.; Li, C. On the modification of hydration resistance of CaO with ZrO2Additive. *Int. J. Appl. Ceram. Technol.* **2016**, *13*, 1173–1181. [CrossRef]
15. Wu, H.; Li, D.; Guo, N. Fabrication of integral ceramic mold for investment casting of hollow turbine blade based on stereolithography. *Rapid Prototyp. J.* **2009**, *15*, 232–237. [CrossRef]
16. Wu, H.; Li, D.; Tang, Y.; Sun, B.; Xu, D. Rapid fabrication of alumina-based ceramic cores for gas turbine blades by stereolithography and gelcasting. *J. Mater. Process. Technol.* **2009**, *209*, 5886–5891. [CrossRef]
17. Lu, Z.; Miao, K.; Zhu, W.; Chen, Y.; Xia, Y.; Li, D. Fractions design of irregular particles in suspensions for the fabrication of multiscale ceramic components by gelcasting. *J. Eur. Ceram. Soc.* **2018**, *38*, 671–678. [CrossRef]
18. Yang, Q.; Zhu, W.; Lu, Z.; Li, D.; Wang, Z.; Wang, F. Rapid fabrication of high-performance CaO-based integral ceramic mould by stereolithography and non-aqueous gelcasting. *Materials* **2019**, *12*, 934. [CrossRef]
19. Hou, Z.; Du, H.; Liu, J.; Hao, R.; Dong, X.; Liu, M. Fabrication and properties of mullite fiber matrix porous ceramics by a TBA-based gel-casting process. *J. Eur. Ceram. Soc.* **2013**, *33*, 717–725. [CrossRef]
20. Hua, Z.; Yao, G.; Ma, J.; Zhang, M. Fabrication and mechanical properties of short ZrO2 fibres reinforced NiFe2O4 matrix composites. *Ceram. Int.* **2013**, *39*, 3699–3708. [CrossRef]
21. Yang, F.; Zhang, X.; Han, J.; Du, S. Mechanical properties of short carbon fibres reinforced ZrB2-SiC ceramic matrix composites. *Mater. Lett.* **2008**, *62*, 2925–2927. [CrossRef]
22. Zhang, Y.; Li, S.; Han, J.; Zhou, Y. Fabrication and characterization of random chopped fibres reinforced reaction bonded silicon carbide composite. *Ceram. Int.* **2012**, *38*, 1261–1266. [CrossRef]
23. Tang, S.; Hu, C. Design, preparation and properties of carbon fibres reinforced ultra-elevated temperature ceramic composites for aerospace applications: A review. *J. Mater. Sci. Technol.* **2017**, *33*, 117–130. [CrossRef]
24. Liu, H.-Y.; Hou, X.-Q.; Wang, X.-Q.; Wang, Y.-L.; Xu, D.; Wang, C.; Du, W.; Lu, M.-K.; Yuan, D.-R. Fabrication of high-strength continuous zirconia fibers and their formation mechanism study. *J. Am. Ceram. Soc.* **2004**, *87*, 2237–2241. [CrossRef]